Influence of Cu Addition on the Wear Behavior of Eutectic Al-12.6Si Alloy Developed by Spray Forming Method

Dayanand M. Goudar , Julfikar Haider , Rajashekar Kurahatti , Rajashekar V. Kurahatti , Deesy G. Pinto *

Posted Date: 23 January 2024

doi: 10.20944/preprints202401.1648.v1

Keywords: Eutectic Al-Si alloy; Spray forming; Microstructure; Hardness; Friction; Wear.

Article

Influence of Cu Addition on the Wear Behavior of Eutectic Al-12.6Si Alloy Developed by Spray Forming Method

Dayanand M. Goudar [1], Julfikar Haider [2], K. Raju [3], Rajashekar V. Kurahatti [4] and Deesy G. Pinto *[5,6]

[1] Department of Mechanical Engineering, Tontadarya College of Engineering, Gadag, India – 582 101; dmgoudartce @gmail.com
[2] Department of Engineering, Manchester Metropolitan University, Manchester, United Kingdom; j.haider@mmu.ac.uk
[3] Department of Mechanical Engineering, St. Joseph Engineering College, Mangaluru, India – 575 028, rajuk@sjec.ac.in
[4] Department of Mechanical Engineering, Basaveshwar Engineering College, Bagalkot,India-587101, rajuk@sjec.ac.in
[5] Department of Civil Engineering and Geology, University of Madeira, Campus da Penteada, Funchal, Portugal-9020-105, deesy.pinto@staff.uma.pt
[6] CQM-Centro de Química da Madeira, Universidade da Madeira, Campus da Penteada, 9020-105, Funchal, Portugal, deesy.pinto@staff.uma.pt
* Correspondence: deesy.pinto@staff.uma.pt

Abstract: The principal main of this research work was the study the influence of Cu addition on the wear behavior (WB) of eutectic Al-12.6Si alloy developed by spray forming (SF) method and compared with as-cast (AC) alloys. The phases of chemical compositions and microstructure were studied by optical microscopy, energy dispersive spectroscopy (EDS) and Scanning Electron Microscopy (SEM). The microstructure of SFAl-12.6Si (SF1) alloy reside — of fine primary and eutectic Si phases evenly distributed in the equiaxed α-Al matrix and SF Al-12.6Si-2Cu (SF2) alloy lie of uniformly distributed fine eutectic Si particulates and spherical form θ-Al2Cu precipitates in α-Al matrix. On other hand, the AC Al-12.6Si alloy (AC1) alloy involve of eutectic Si needles in the dendrite α-Al matrix, whereas AC Al-12.6Si-2Cu (AC2) alloy consisted of eutectic Si needles and Chinese script form θ phase distributed randomly in the α-Al matrix. The microhardness and wear properties were analyzed using Vickers hardness (VH) and dry sliding WT. The SF alloys exhibit superior hardness compared to the AC alloys. The wear properties of SF alloys exhibited significantly superior compared to the AC alloys. The SF2 alloy showed high wear resistance (WR) than the SF1 alloy in the entire sliding velocities and applied loads. The results indicate that the spray deposited alloys have a lower coefficient of friction (CF(μ)) than the AC alloys under varying load and sliding velocity conditions. The high WR in the SF alloy was due to microstructural modification during SF and precipitation of fine Al2Cu intermetallic and solid solubility effects. The SF2 depicts increased transition from oxidative to abrasive. In other ways, AC alloys demonstrate wear mechanisms that change from oxidative to abrasive and delamination with an increase in sliding velocity and load.

Keywords: Eutectic Al-Si alloy; Spray forming; Microstructure; Hardness; Friction; Wear

1. Introduction

Cast aluminum alloys are widely used in various industries, such as chemical vessels, aircraft, and automotive, due to their lightweight nature, high strength, and excellent wear and corrosion resistance [1-3]. The most significant cast aluminum alloy system is the aluminum-silicon (Al-Si) alloy. Increase in the silicon content (4-13%), which helps to produce excellent casting properties [4]. TheAl-Si eutectic alloy is about a cast structure made primarily of acicular/needle-shaped eutectic Si phases that are randomly distributed throughout the dendritic α-Al matrix. When we proceed with

 doi:10.20944/preprints202401.1648.v1

the modification of the morphology of Si particles from a needle/rod-like shape to a nearly spherical/equiaxed, it is possible to improve their WR. This modification can result in stronger bonding between the matrix and the particle, and it can reduce the stress concentration caused by needle/rod-shaped Si particles [5-8]. Several studies have been conducted to examine the impact of silicon particles on WB. However, only a limited number of studies have focused on determining how the shape, size, and distribution of Si particles affect the dry sliding WB of Al-Si alloys. Riahi et al. [9] considered the effect of silicon particle morphology on the WB of Al-Si alloys, while Elmadagli et al. [10] did a comprehensive investigation to establish the correlation between microstructure and WB in Al-Si alloys. Their obtained results suggest that silicon particles with lower aspect ratios exhibit improved WR and shown that reducing the aspect ratio of the Si phase in an Al-Si alloy can improve its WR [11]. To further enhance WR, Liu et al. recommend having uniformly distributed, finely spherical Si particles [12]. However, some studies have found that hypereutectic Al-Si alloys with a high Si concentration showed a low wear rate (WRt) and an increased transition load [13]. The addition of certain alloying elements, such as iron, copper, manganese, chromium, magnesium, nickel, and zirconium, can improve the WR of Al-Si alloys at both room and high temperatures. Among these, copper can be particularly effective due to its high solubility in aluminum. When copper combines with aluminum and silicon, it creates a stronger alloy due to the formation of Al2Cu compound, which enhances the WR of the alloy [14-16]. The addition of 1-4% Cu to the eutectic Al-Si alloy increases WR and extends the wear transition period from mild to severe. This is due to the strengthening effects of solid solutions, precipitation hardening, and enhanced matrix hardness.[17]. The Al-Si-Cu alloy has a microstructure that consists of large Si intermetallic phases. These phases increase stress and reduce WR. Furthermore, the intermetallic phase is hard and brittle, which poses a challenge for casting parts. [18]. Tash and Essam found that the θ-Al2Cu intermetallic phase decreased the WRt in Cu-containing Al-Si alloys [19]. Various casting techniques have been used to refine the microstructure of the Al-Si alloy. One of these techniques is SF, which is a rapid solidification process. This process can produce near-net-shape components with a homogeneous microstructure consisting of fine, equiaxed grains. The primary and eutectic Si, as well as the modified precipitates, will appear as fine, globular-shaped particulates [20]. The numerous studies was carried out on the wear characteristics of Al-Si alloys manufactured through SF with varying amounts of Si. The obtained results showed that these alloys had superior wear performance compared to those manufactured through conventional casting methods. Additionally, the addition of Cu and Mg as alloying elements in SF Al-Si alloys resulted in even lower WRts than in the binary Al-Si alloys [21]. Insufficient research exists on the tribological characteristics of the SF eutectic Al-Si alloy with Cu addition. The present study aims to examine the microstructural properties and wear characteristics of both Al-12.6 and Al-12.6-2Cu alloys produced by the SF technique and compare them to their AC counterparts. The findings of this study will provide valuable insights into the influence of Cu on the tribological properties of the Al-Si alloy. The results will be useful for researchers, industry professionals, and stakeholders in developing improved materials for tribological applications.

2. Materials and Methods

The Al-12.6Si and Al-12.6Si-2Cu alloys were prepared from the master alloys of Al (99.7%), Al-20Si and Al-50Cu alloys. Table 1 shows the chemical composition of the alloys. The SF process was used to produce the Al-12.6Si (SF1) and Al-12.6Si-2Cu (SF2) alloys; and the details of the SF process have been described elsewhere [22,23]. Table 2 shows the list of the process parameters employed in the current work. A free fall atomizer was employed to atomize the superheated liquid metal stream by using nitrogen gas. The flow diagram of the SF process is depicted in Fig.1.

Table 1. The details of the experimental alloys' composition (wt.%).

Alloy	Si	Fe	Mn	Mg	Cu	Ni	Al
Al-12.6Si (AC1)	12.6	0. 3	0.06	0.24	0.04	---	Bal.
Al-12.6Si-2Cu (AC2)	12.6	0. 4	0.02	0.14	2.06	--	Bal.

 doi:10.20944/preprints202401.1648.v1

Table 2. Particulars of process parameters in Spray forming.

Variable	Value
Melt Superheat	150°C
Melt rate	2.8 kg/min kg/min
Gas pressure	0.55 MPa
Diameter of nozzle	4.0 mm
Deposition distance	400 mm

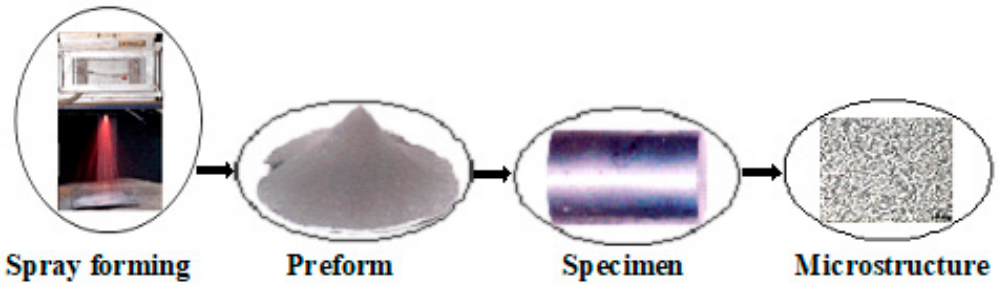

Figure 1. Flow diagram depicting the details of Spray forming.

The AC and secondary processed SF Al–12.6Si and Al–12.6Si–2Cu alloys microstructure samples were prepared by standard metallographic techniques and etched with Keller's reagent. The microstructural features were studied under an Optical Microscope and SEM. The hardness measurement was carried out on an HV-5 VH Tester at a load of 300 g and a dwell period of 15s as per ASTM: E384-11e1. The dry sliding wear testing was carried out on a pin-on-disk tribometer as per ASTM: G99-05. The disk was made of EN-32 steel with a hardness of 65HRC. The wear specimens were of size Ø8 x 30 mm and were polished and cleaned with acetone before being tested. The wear tests (WT) were performed at different loads ranging from 10 to 40 N for a sliding distance of 2000 m at sliding velocities of 1, 2 & 3 m/s. The topographical features of worn-out surfaces were analysed using SEM.

3. Results and Discussion

3.1. Porosity measurement

Porosity has been observed to be an inevitable entity in SF alloys. However, depending on the location and processing parameters, its proportion, and features in the preform change. The porosity heavily influences the mechanical, wear and corrosion properties of the alloys. In the current investigation, hot pressing was used for porosity reduction in the alloys. The porosity values reported are shown in Table 3. In comparison to SF1 alloy, SF2 alloy has less porosity after hot compaction. The variation in monitoring the process parameters in SF may be the cause for the variation in porosity in alloys before hot compaction. The increasing preforms surface's heat condition during deposition has a significant effect on the porosity's nature and amount. As a result, minimizing pre-form porosity requires careful control of processing parameters. Many researchers have investigated how porosity develops during SF [24]. The high liquid fraction in the spray typically causes gas to become trapped within the liquid, resulting in spherical holes. The SF1 alloy had a high porosity than SF2 alloy before hot compaction. This can be because the spray contains a significant amount of liquid. In the spray deposited alloys, the porosity was significantly reduced by hot compaction.

 doi:10.20944/preprints202401.1648.v1

Table 3. Porosity values of spray formed alloys.

Particulars	SF1 alloy	SF2 alloy
Theoretical density (gm/cc)	2.65	2.78
Density before hot pressing (gm/cc)	2.17	2.33
Density after hot pressing (gm/cc)	2.46	2.64
% porosity before hot pressing	18%	16%
% porosity after hot pressing	7%	5%

3.2. Microstructural features of Al-Si alloys

The optical and SEM microstructures of the AC1 alloy are shown in Fig. 2(a) & 2(b). It consists of eutectic Si needles dispersed randomly throughout the α-Al matrix. The EDX spectrum of AC1 alloy is shown in Fig. 2(c). The Al and Si peaks in the spectrum are particularly prominent. As shown in Fig. 3(a), the SF1 alloy microstructure was composed of evenly dispersed, fine eutectic Si particulates. Figure 3(b) depicts the BSED image of the SF1 alloy, in which the fine Si particles are uniformly dispersed throughout the α-Al matrix. The EDX spectrum of the SF1 alloy made of Al and Si is shown in Fig. 3(c). Additionally, it was found that the matrix included 7 vol.% of micron-sized porosity and had an improved solid solubility of Si. The high fraction of liquid in the spray causes the entrapment of gas in the liquid, which results in the formation of pores in the alloys [24]. However, the amount of porosity was not influenced significantly by the presence of Cu and Si.

The SEM and elemental distribution of the AC2 alloy are shown in Fig. 4(a)-(d). The random distribution of the eutectic Si phase, the Chinese script form of θ-Al2Cu, and the Q-Al-Si-Cu phases in the dendritic α-Al matrix. At the grain boundaries of the Al dendrite arms, the intermetallic θ and Q phases were found as coarse Chinese-script/vermiform ranging in size from 50 to 170 μm. Table 4 displays the composition of the AC2 alloy as determined by EDS/EDX analysis.

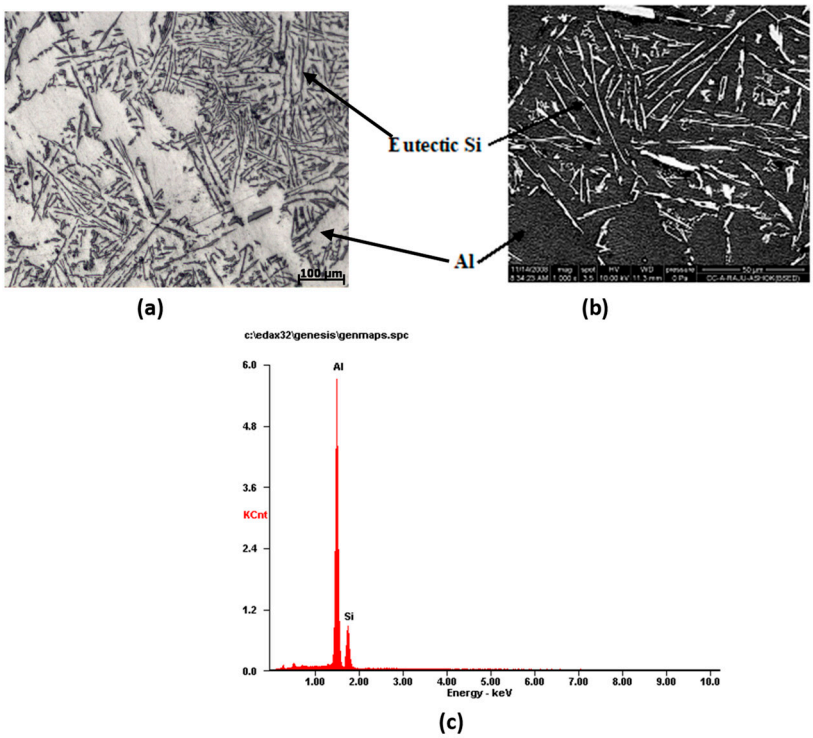

Figure 2. AC1 alloy (a) Optical microstructure (b) BSED image (c) EDX Spectrum.

Preprints.org (www.preprints.org) | NOT PEER-REVIEWED | Posted: 23 January 2024 doi:10.20944/preprints202401.1648.v1

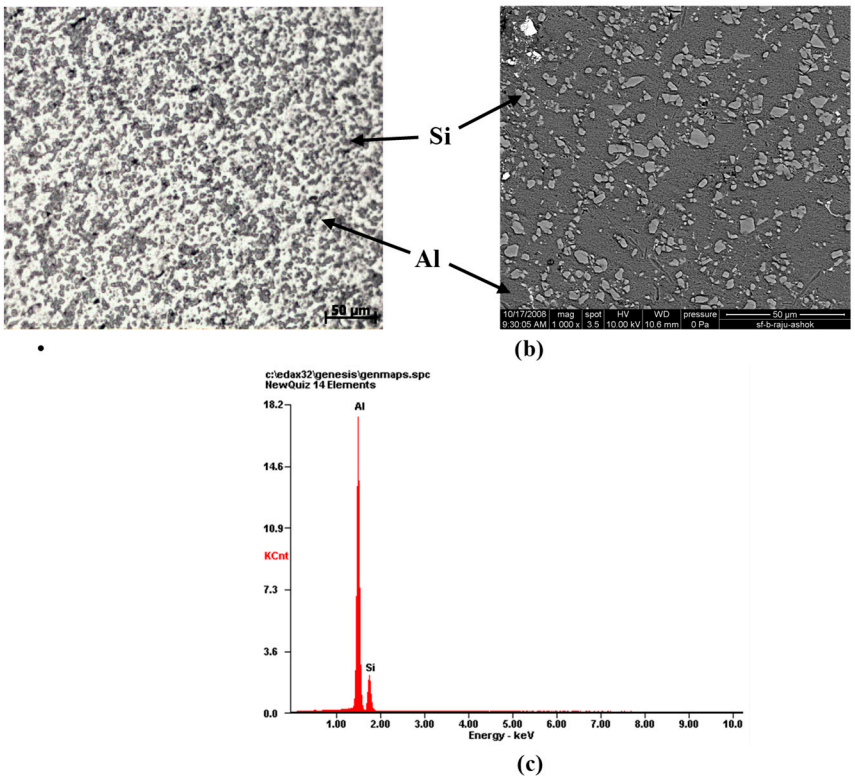

Figure 3. SF1 alloy (a) Optical microstructure (b) BSED image (c) EDX Spectrum.

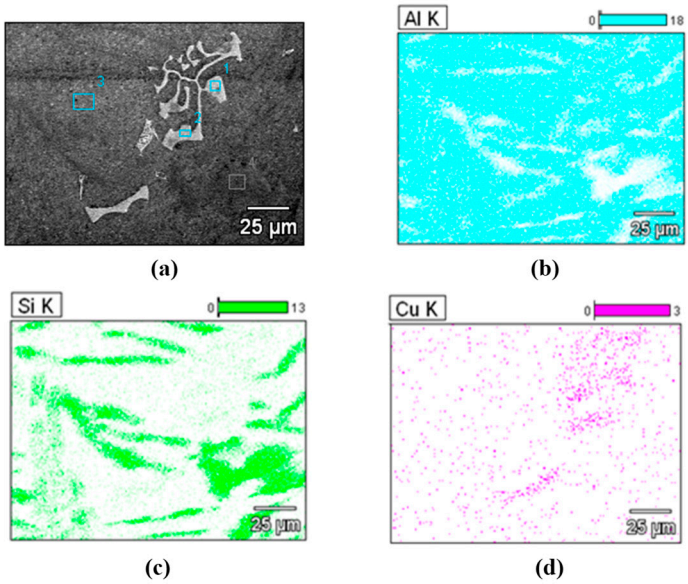

Figure 4. (a) SEM micrograph of AC2 alloy & elemental mapping of (b) Al, (c), Si and (d) Cu. * The numbers in Fig. 4(a) indicate the EDS/EDX spot position

Table 4. Phase composition of AC2 alloy by EDS/EDX analysis.

EDX spots	Phase	Al-K	Fe-K	Si-K	Cu-K
Spot 1	Q-Al74Si9Cu10	65.88	0.89	8.02	26.43
Spot 2	θ-Al2Cu	67.23	0.30	1.97	30.50
Spot 3	α-Al	97.81	0.41	0.24	0.00

 doi:10.20944/preprints202401.1648.v1

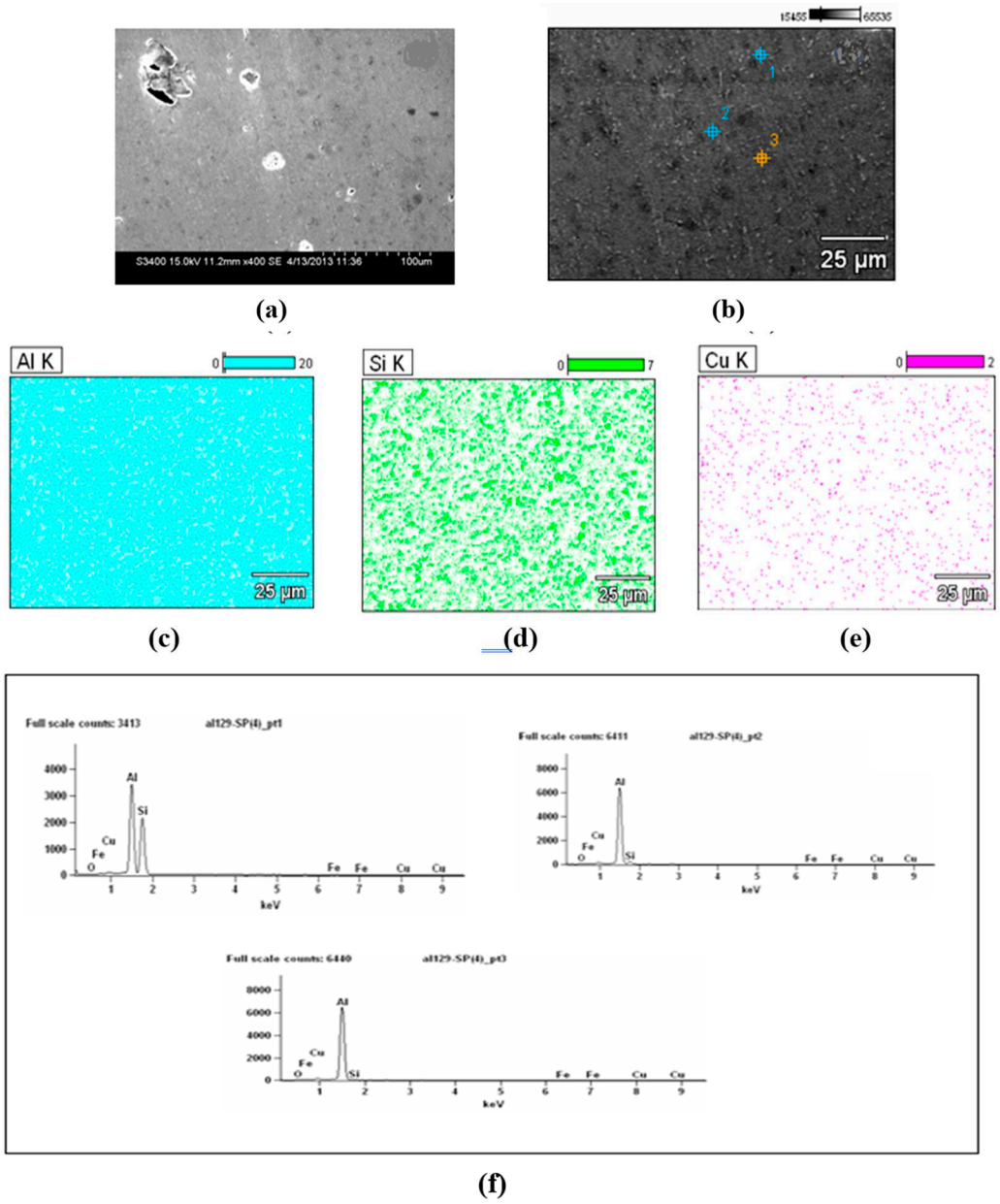

Figure 5. (a) SEM Micrograph of hot-compressed SF2 alloy (b) EDS micrograph (c) elemental mapping of Al (d) mapping of Si (e) mapping of Cu (f) EDS spectra of eutectic Si, Q and α-Al phases.

Table 5. Phase composition of SF2 alloy by EDS/EDX analysis.

EDX spots	Phase	Al-K	Si-K	Fe-K	Cu-K
Pt1 - Eutectic Si	$Al_{48}Si_{51}$	45.72	50.13	0.89	1.57
Pt2 - Q-phase	$Al_{93}Si_6Cu_{1.9}$	89.02	6.99	0.30	2.09
Pt3 - α(Al)	$Al_{92}Si_1$	92.89	1.27	0.41	3.62

Figure 5(a) depicts the SEM micrograph of the SF2 alloy. The microstructure of the alloy showed fine precipitates of θ-Al2Cu and Q-phases in an equiaxed Al matrix, as well as a uniform, homogenous distribution of fine eutectic Si particles with sizes ranging from 3 to 7 µm. Additionally, 5 vol% of spherical micropores that were randomly distributed were noted. The EDS analysis of the SF2 alloy has revealed fine eutectic Si, fine precipitates of θ-Al2Cu, and Q-Al74Si9Cu10 phases in the alloy. Table 5 displays the composition of phases. After being hot pressed, the microstructure of the SF2 alloy (Fig. 5(b)) showed eutectic Si and θ phase fragmentation. Additionally, the increase in the volume percentage of Si phases, a decrease in porosity, and homogeneous Al-matrix were observed.

 doi:10.20944/preprints202401.1648.v1

The fine θ and Q-intermetallic compounds began to precipitate at room temperature as a result of the alloy's rapid cooling during the atomization and deposition process, which kept all of the solute in a supersaturated state. Figures 5 (c), (d) & (e) display the elemental mapping and Figure 5(f) depicts the EDS spectra of Si, Q and α-Al phases of hot-compressed SF2 alloy.

3.3. Hardness

Table 6 displays the micro-hardness values of the AC and SF alloys. In comparison to AC alloys, the results show a considerable increase in the microhardness of SF alloys. The hardness of the SF1 alloy is 36% greater than that of the AC1 alloy, while the SF2 is 33% higher than the AC2 alloy. The SF2 is invariably 41% harder than AC1 alloy. The small and hard Si particles that are uniformly dispersed throughout the Al matrix and that resist localized deformation when the indentation is applied may be the cause of the high hardness of the spray-deposited alloys. The plastic deformation was significantly hampered by the fine eutectic Si phase. The SF2 alloy high hardness may be attributed to the fine precipitation of hard Al2Cu intermetallic phase distributed uniformly throughout the Al matrix and a higher volume fraction of eutectic Si, which causes an obstruction in the indentation and raises the hardness [21]. Additionally, the SF process's rapid solidification, which produced more fine precipitates and a hardening effect, may have contributed to the increased hardness that resulted by adding another barrier to the dislocation motion [25].

Table 6. Hardness values of as-cast and spray formed alloys.

Alloy	Hardness (Hv)
AC1	43±4.1
AC2	48±3.2
SF1	67±5.1
SF2	73± 4.5

3.4. Wear characteristics

3.4.1. Variation of wear rate with load at constant sliding velocity

The WRts of both AC and SF alloy are shown in Fig. 6(a)-(c). The alloys were tested for wear at sliding velocities of 1, 2, and 3 ms-1, with a sliding distance of 2000 m and a load range of 10–40 N. The results show that the WRt increases for all alloys as the load is increased, regardless of the type of alloy or sliding velocity. Additionally, it was observed that AC alloys consistently have a higher WRt than SF alloys. Among the tested alloys, the SF2 alloy has the lowest WRt , while the AC1 alloy has the highest WRt across the whole range of applied load and sliding velocity.

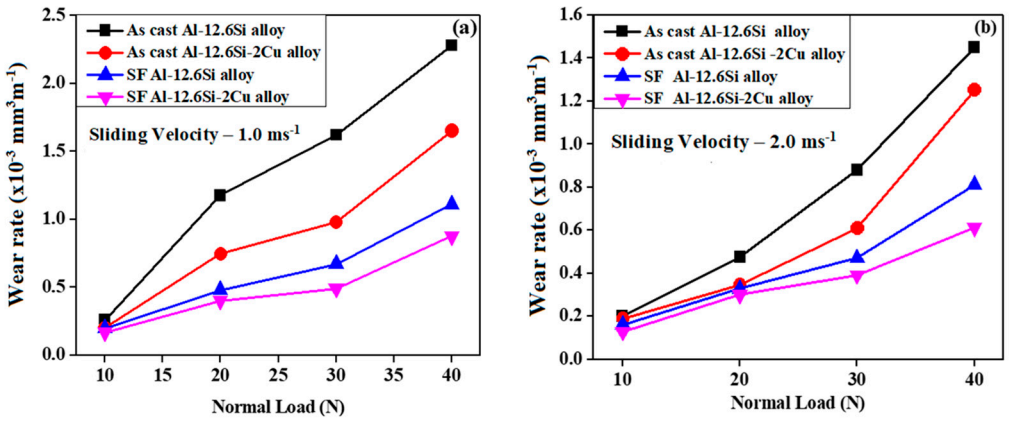

 doi:10.20944/preprints202401.1648.v1

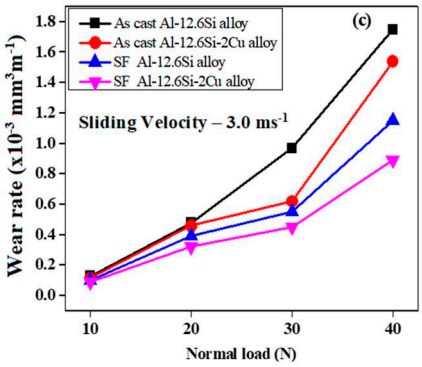

Figure 6. The variation of the WRt of AC and SF alloys as a function of normal load and sliding velocity (a) 1.0 ms^{-1} (b) 2.0 ms^{-1} and (c) 3.0 ms^{-1}.

During wear testing, the long eutectic Si needles tend to break more frequently than the tiny Si particles. This is due to an increase in the alloy's shear stress as the load increases, which results in easier fracturing of the eutectic Si and deformation of the matrix around it. The size of the eutectic Si may influence the stress concentration caused by deformation, with the interface between Si needles and the α-Al matrix being more susceptible to this effect than the interface between tiny Si particles and the α-Al matrix. In the present study, this was observed as coarse eutectic Si fractured easily, leading to decreased WR of the ACalloys. However, in spray deposition, the eutectic Si is more finely divided and evenly dispersed throughout the α-Al matrix. The AC2 and SF2 alloys have a higher WR than AC1 and SF1 alloys. This is because of the presence of the θ phase in ternary alloy. The strengthening effect of the θ phase on the α-Al matrix lowers the possibility of Si needles peeling off from the matrix, decreasing the WRt . The secondary processed SF2 alloy has better WR than AC2 alloy. This is because of the uniform distribution of refined eutectic Si and fine precipitates of Chinese script like θ-Al2Cu intermetallic phases in the α-Al matrix. The Si and θ phases in the alloy have been further finely refined by hot compaction, decreasing the WRt of the alloy [22]. The WRt of AC and SF alloys is low at low load (10 N) and low sliding velocity (1.0 ms-1), with no appreciable variation between the alloys (Fig. 6a). There will be less contact between the mating surfaces and at low contact pressure, the interface temperature is adequate to produce metal oxide film, which will be removed off the pin surface during sliding. Therefore, oxidative wear was responsible for the separation of the oxidized film between the mating surfaces and the removal of oxides from the interface. The clear sign of a change in the WB was the rise in WRt as the applied load increased (from 10 to 20 N). The slope of the WRt versus applied load has been observed to increase at higher applied loads (more than 20 N). This demonstrates that the wear process has switched from mild oxidative-metallic wear to delamination pure metallic wear. At a high load, the sliding surface is subjected to high shear stress, which causes cracks and spreads beneath the plastically deformed surface and may eventually cause the alloy to delaminate from the surface. This underlying wear process causes the WRt to increase with the load [26]. For both the SF and AC alloys, WRts increased at 40N load.

3.4.2. Variation of wear rate with sliding velocity at constant applied load

 doi:10.20944/preprints202401.1648.v1

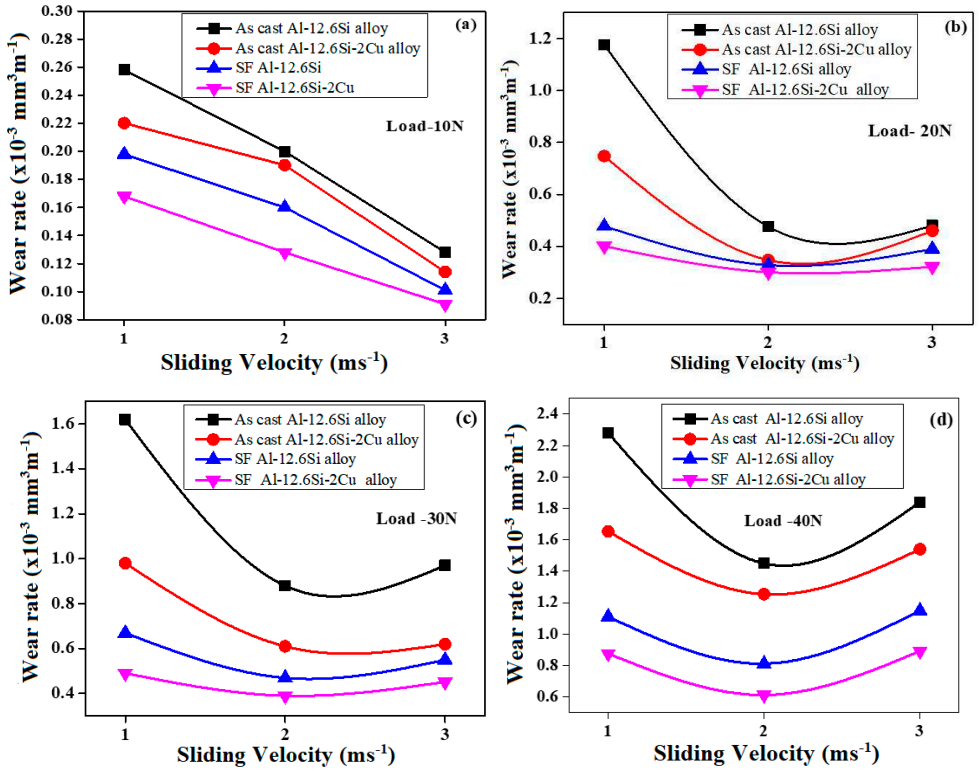

Figure 7. Variation of WRt with sliding velocity at a load of (a) 10 N(b)20 N(c) 30 N (d) 40 N.

Understanding how the WRt changes with sliding velocity at a constant load is crucial (refer to Fig. 7a-d). At a low load of 10 N, the WRt decreased as the sliding velocity increased (Fig. 7a). Initially, the wear rate was high at a low sliding velocity of 1.0 ms-1. The lowest WRt was found at 2.0 ms-1 for loads of 20 N and 30 N, and beyond this point, the WRt increased somewhat at higher sliding velocities (Fig. 7b & 7c). However, at a high load of 40 N, the lowest measured WRt was at a sliding velocity of 2.0 ms-1, and beyond this point, the WRt significantly increased (Fig. 7d). During the friction force, a metal oxide layer forms on the pin surface, which then gets removed during the sliding process. Therefore, at low loads, only oxidative wear takes place. At a higher load of 40N, adhesive wear takes over, where severe plastic deformation of the surface occurs. This causes a higher interface temperature, which then heats the worn surface and softens the matrix. Furthermore, the worn surface experiences greater penetration and plastic deformation. As a result, both the AC and SF alloys experienced mixed adhesive and abrasive wear at higher loads. As per the study [27], it has been observed that the WRt decreases as the sliding speed increases up to a critical sliding velocity (2.0 m/s) . However, as the sliding speed increases beyond 2.0 m/s, the WRt starts to increase. This happens because the reduced surface contact between the pin and disc leads to lower WRts at first, but the increase in sliding velocity raises the strain rates, improves the flow strength, and increases the flow rates, which eventually increases the WRt [28]. Moreover, at higher sliding velocities (between 2 and 3 m/s), the interface temperature increases due to the rise in friction heat, which makes the alloy softer. This leads to more surface contact, resulting in a higher WRt [29]. During the SF process, the rapid solidification of alloys led to the development of fine eutectic Si, an increase in the volume fraction of the Si phase, and an increase in the solid solubility of Si in the matrix. This process reduced the stress concentration at the interface between the fine and spherical Si phase and the equiaxed Al matrix, which lowers the likelihood of subsurface cracks forming. Additionally, the strong interface bond strength with the matrix may improve the WR of the SF alloys. Cu addition has improved the thermal stability of Al-Si alloys by generating a hard θ-Al2Cu intermetallic compound in the Al matrix. This resulted in an increase in the transition period for both SF and AC alloys, leading to mild to severe WRt. In the SF2 alloy, the development of fine θ-Al2Cu intermetallic precipitates was coherent with the soft Al-matrix, which increased the hardness and WR by resisting

 doi:10.20944/preprints202401.1648.v1

dislocation motion. However, the presence of extremely hard, coarse, and brittle θ-Al2Cu intermetallic phase, as well as the needle-like eutectic Si phase, in the α-Al matrix, resulted in high WRt in AC2 alloy. This faceted structure of intermetallic and Si phases existed as discrete particles that had a relatively weak bond with the matrix and served as stress raisers. The eutectic Si and hard intermetallic phases were also anticipated to have the potential for crack nucleation [30].

3.4.3. Variation of friction coefficient with load at constant sliding velocity

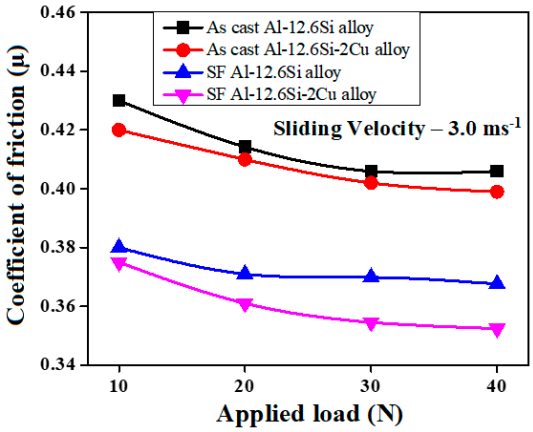

Figure 8. Coefficient of friction versus applied load at a sliding velocity of 3.0 ms-1.

In Figure 8, the relationship between the CF(μ) and the applied load at a sliding velocity of 3.0 ms-1 is presented. It was observed that the CF(μ) remained almost steady with a slight decrease over time as the load increased. The results indicate that regardless of the composition, the SF alloys had a lower CF(μ) than the ACalloys. The AC2 alloy, in particular, had the lowest CF(μ). At a load of 10N, the SF1 and SF2 alloys had 7% and 4% less CF(μ) , respectively, compared to the AC alloys. At a high load of 40N, the CF(μ) of SF1 and SF2 alloys was 9% and 6% less than the AC1 andAC2 alloys, respectively. When the load is low, there is no metal-to-metal contact between the pin and counter surface. Instead, the behavior is influenced by the oxidation process and the adhesion of small protrusions on the contacting surfaces. As the load increases, the CF(μ) decreases slightly, which may be because of metallic contact between the counter face and the pin. This contact leaves no room for imperfections and locks the surface contact area. The slight variation in the CF(μ) at higher loads may be attributed to the fact that all alloys have more aluminum than the alloying elements. At higher loads, the aluminum matrix in the specimens and the counter face come in contact with each other, which determines the effective CF(μ) .

3.5. Topographical features of worn surfaces

The worn surfaces of AC and SF alloys at 40 N load and sliding velocity of 3.0ms-1 as shown in figure 9. The topography of the worn surfaces indicates that the binary alloys have suffered more damage than the ternary alloys. The worn surface of the AC1 showed several features including oriented overlapping flaky structures, wear scars, craters, crass plastic flow of metal, metallic fracture of ridges, and edge cracking (see Fig. 9(a)). The damaged surface also revealed evident signs of plastic deformation along with adhesive wear. On the other hand, the AC2 alloy as shown in Fig. 9b depicts with wide parallel grooves, compacted oxide patches, and a few discontinuous abrasive grooves on its worn surface. During the WT, the sliding of a soft pin surface against a hard disc caused two types of abrasive wear. The first type occurred when the pin penetrated the disc and created continuous parallel grooves. The second type occurred when hard intermetallic phases, such as Si and Al2Cu, were introduced between the sliding surfaces. This type of wear caused the formation of surface cavities due to debris detachment, which indicated delimitative wear on the surface layers. As a result, cracks formed below the surface layers and grew until they joined together, forming plate-shaped particles that detached from the wearing surface.

 doi:10.20944/preprints202401.1648.v1

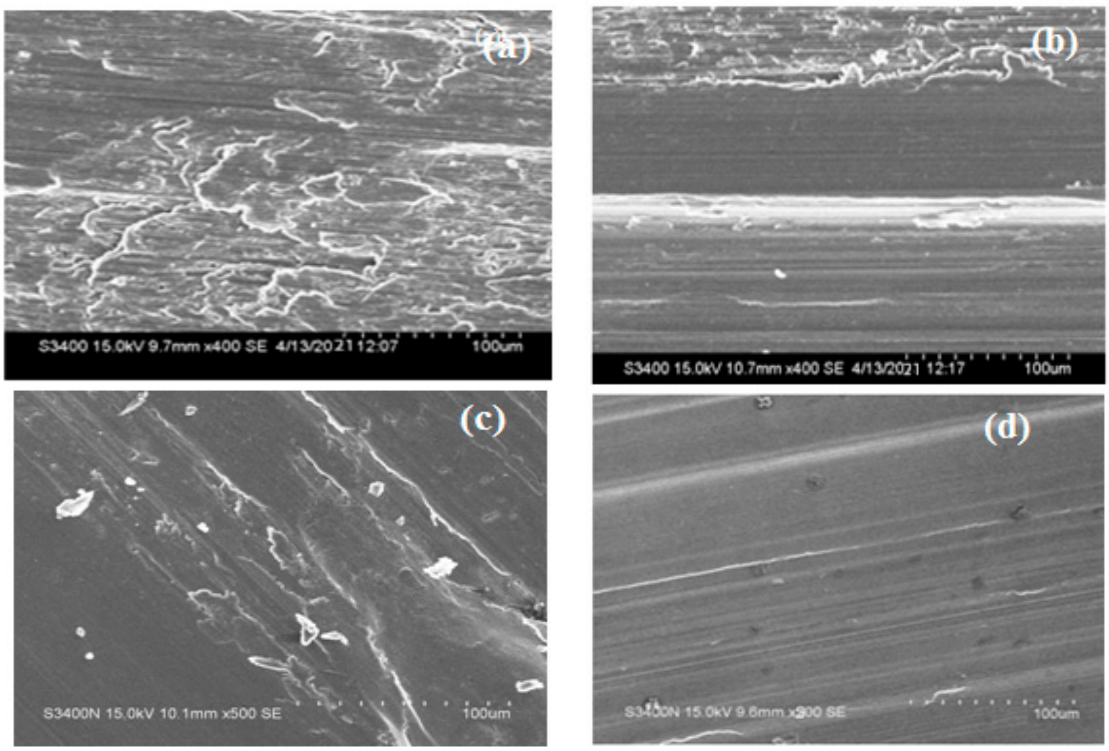

Figure 9. SEM micrographs of worn surfaces of (a) AC2 (b) AC2 (c) SF1 and (d) SF2 alloys**.**

In Figure 9(c), we can observe the worn surface of SF1, which displayed a homogenous wear pattern. The surface was smooth with fine abrasion grooves, a few small dimples, and some scoring marks that extended from end to end. Additionally, the surface showed white patches, indicating the early stages of oxide formation. On the other hand, in Figure 9(d), we can see the worn surface of SF2 alloy, which had small, homogeneous, and continuous grooves. The surface was smooth with fine scoring marks, and it had no pits or dimples, indicating a low WRt [22].

4. Conclusions

- The microstructure of SF1 consists of eutectic Si particles ranging from 4 to 7 μm are uniformly distributed in the Al-matrix. The SF2 alloy exhibited a uniform distribution of eutectic Si, Al2Cu and Al-Si-Cu intermetallic phases in the equiaxed Al-matrix.
- The SF2 alloy exhibits superior WR than the AC alloys under varying load and sliding velocity conditions. Specifically, at a 40 N load, the WR of the SF2 alloy is 62%, 47%, and 23% higher than the AC1, AC2, and SF1 alloys, respectively, when sliding at 1 m/s. Similarly, when sliding at 3 m/s, the WR of the SF2 alloy is 52%, 42%, and 21% higher than the AC1, AC2, and SF1 alloys, respectively.
- The primary wear mechanism for the AC alloys under dry sliding conditions, involved abrasion, adhesion and SF alloys involved oxidation and abrasion. The increased load resulted in more wear due to the increased depth of penetration. However, at 40N for all sliding velocities, the AC alloys exhibited considerably higher wear loss throughout the sliding distance compared to SF alloys. This was attributed to the softening of the wearing pin at the high load, which accelerated both abrasive and adhesive wear at 3.0m/s sliding velocity.
- The SF2 alloy exhibited a lower WRt compared to the SF1 alloy at all applied loads and sliding velocities. This improvement was attributed to fine and uniform distribution of Si and intermetallic and increased solid solubility. This section may be divided by subheadings. It should provide a concise and precise description of the experimental results, their interpretation, as well as the experimental conclusions that can be drawn.

Author Contributions: D.M.G.— obtained the mechanical, wear, phases of chemical compositions, microstructure and hardness results and did data processing. JH, RVK and KR - helped with the collection from

the scientific literature review about the subject, organization of obtained results from the scientific community, contribution for the discussion of the selected results; D.M.G, JH, RVK, KR and DGP - helped with results interpretation, manuscript writing. All authors have read and agreed with the contents of the manuscript and there is no financial interest to report. We certify that the submission is original work and is not under review at any other publication.

Funding: The authors gratefully acknowledge the financial support received for this work from Vision Group on Science and Technology (VGST), Government of Karnataka, Bengaluru under the scheme VGST/K-FIST (LEVEL–I)/GRD-885.

Acknowledgements: Deesy Pinto wishes to express a sincere acknowledgement to Fundação para a Ciência e a Tecnologia (FCT) with Portuguese Government funds through the CQM Base Fund - UIDB/00674/2020 (DOI: 10.54499/UIDB/00674/2020) and Programmatic Fund - UIDP/00674/2020 (DOI 10.54499/UIDP/00674/2020) and by ARDITI-Agência Regional para o Desenvolvimento da Investigação Tecnologia e Inovação through funds from Região Autónoma da Madeira-Governo Regional.

Conflicts of interest: The authors declare no conflict of interest.

Acronyms

AC-as-cast; CF(μ) - coefficient of friction; EDS - Energy Dispersive Spectroscopy;

WB - Wear behavior; WT – Wear test(s); WRt(s) - Wear rate (s); WR - Wear Resistance; SF - Spray Forming; SEM - Scanning Electron Microscopy; VH - Vickers hardness.

References

1. M.A. Awotunde, A.O. Adegbenjo, B.A. Obadele, et al., J Mater Res Technol. 8, 2432 (2019) https://doi.org/10.1016/j.jallcom.2021.163321
2. A.M. Ali, M.Z. Omar, H. Hashim et al., Rev Adv Mater Sci. 60, 801 (2021) https://doi.org/10.1515/rams-2021-0062
3. B. Abbasipour , B. Niroumand, S.M. M. Vaghefi et al., Tribological behavior of A356–CNT nanocomposites fabricated by various casting techniques, T Nonferr Metal Soc. 29, 1993–2004 (2019) https://doi.org/10.1016/S1003-6326(19)65107-1
4. X. Zhuo, Q. Zhang, H. Liu et al., Journal of Alloys and Compounds. 899, 163321 (2022). https://doi.org/10.1016/j.jallcom.2021.163321
5. Y. Wu, C. Liu, H. Liao et al., J Alloys Compd. 856, 158072 (2021), https://doi.org/10.1016/j.jallcom.2020.158072
6. S. Liu, X. Zhang, H.L. Peng et al., J Mater Res Technol. 9, 4644 (2020), https://doi.org/10.1016/j.jmrt.2020.02.091 747
7. A.A. Rahman, M.S. Salleh, I.S. Othman et al., J Adv Manuf Technol. 14, 1 (2020), https://jamt.utem.edu.my/jamt/article/view/6029
8. Gencaga Purcek, Onur Saray and Oktay Kul, Met. Mater. Int. 16, 145 (2010), https://doi.org/10.1007/s12540-010-0145-1
9. A.R. Riahi, and A.T. Alpas, Mat Sci Eng A. 44, 326 (2006) DOI: 10.1016/j.msea.2006.08.043
10. M. Elmadagli, T. Perry and A.T. Alpas, Wear. 262, 79 (2007) DOI: 10.1016/j.wear.2006.03.043
11. Parveen Kumar and M. F. Wani, Jurnal Tribologi.15, 21 (2017) https://www.jurnaltribologi.mytribos.org/v15/JT-15-21-49.pdf
12. Gang Liu, Guodong Li, Anhui Cai and Zhaoke Chen, Materials & Design. 32, 121 (2011), http://dx.doi.org/10.1016/j.matdes.2010.06.027
13. F. Alshmri, H.V. Atkinson, Sarah V Hainsworth and C. Haidon, Wear. 313 (2014) DOI: 10.1016/j.wear.2014.02.010
14. Luis Antonio de Souza Baptista, Kessia Gomes Paradelaa, Ivaldo Leão Ferreira, Amauri Garcia and Alexandre Furtado Ferreira, Mater. Res. Technol. 8, 1515 (2019), https://doi.org/10.1016/j.jmrt.2018.05.021
15. Yan Zheng, Wenlong Xiao, Sujing Ge, Weitao Zhao, Shuji Hanada and Chaoli Ma, Journal of Alloys and Compounds. 649, 291 (2019) DOI: 10.1016/j.jallcom.2015.07.090
16. Giulio Timelli, Alberto Fabrizi, Simone Vezzù and Alessandro De Mori, Metals. 10, 1 (2020)
17. Muzaffer Zeren, Erdem Karakulak and Serap Gümüş, Influence of Cu addition on microstructure and hardness of near-eutectic Al-Si-xCu-alloys, Transactions, 21, 1698-1702 (2011), https://doi.org/10.1016/S1003-6326(11)60917-5
18. Wen-Chi Chen, Chih-Ting Wu, Hui-Yun Bor, and Sheng-Long Lee, Journal of Materials Engineering and Performance. 22, 3854 (2013), DOI:10.1007/s11665-013-0634-8

19. M.T. Mahmoud and R.I.M. Essam, Materials. 9, 442 (2016) DOI: https://doi.org/10.3390/ma9060442
20. Eunkyung Lee and Brajendra Mishra, Effect of Solidification Cooling Rate on Mechanical Properties and Microstructure of Al-Si-Mn-Mg Alloy, Materials Transactions. 58, 1624-1627 (2017) DOI: 10.2320/matertrans.M2017170
21. S.G. Patrick, Solidification in Spray Forming, Metallurgical and Materials Transactions A, 38, 1520-1529 (2017) DOI: 10.1007/s11661-006-9015-3
22. M.G. Dayanand, K. Raju, V.C. Srivastava and G. B. Rudrakshi, Top of FormBottom of FormMaterials & Design., 51, 383 (2013) http://dx.doi.org/10.1016/j.matdes.2013.04.018
23. K. Raju, Effect of processing techniques on the microstructure & wear characteristics of Al-Si alloys, Ph. D. Thesis, IIT(BHU) (2009)
24. Haichao Li, Fuyang Cao, Shu Guo, Yandong Jia et. al., J Alloys and Compounds. 719, 89 (2017) DOI: 10.1016/j.jallcom.2017.05.101
25. W.D. Cai and W.J. Lavernia, Mat. Sci. Eng. A, 8, 226-228 (1997)
26. E.J. Lavernia, N.J. Grant and T. Ando, Rapidly solidified materials (Eds) (Lee PW, Carbonara RS, Ohio, 1986) pp 29 ISBN-13: 978-0871702241
27. W.S. Gwidon, Wear – Materials, Mechanisms and Practice, (John Wiley & Sons Ltd, The Atrium, Southern Gate, Chichester, West Sussex PO19 8SQ, England, 2006), ISBN-13: 978-0-470-01628-2 (HB)
28. Leyu Lin, Yuxiao Zhao, Chi Hua and Alois K. Schlarb, Tribol Lett, 69, 68 (2021), https://doi.org/10.1007/s11249-021-01452-8
29. A.G. James, Metal Transfer and Wear, Front. Mech. Eng., 2020, https://doi.org/10.3389/fmech.2020.00062
30. Cyrus Bidmeshki, Vahid Abouei, Hassan Saghafian et al., Journal of Materials Research and Technology, 5, 250 (2016), http://dx.doi.org/10.1016/j.jmrt.2015.11.008